Piecewise Geodesics for Vessel Centreline Extraction and Boundary Delineation with application to Retina Segmentation

Da Chen and Laurent D. Cohen

CEREMADE, UMR 7534, Université Paris Dauphine PSL*,
75775 Paris Cedex 16, France
{chenda,cohen}@ceremade.dauphine.fr

Abstract. Geodesic methods have been widely applied to image analysis[17]. In this paper, we propose an automatic anisotropic fast marching based geodesic method to extract the centrelines of retinal vessel segments and their boundaries. Our method is related to the geodesic or minimal path technique which is particularly efficient to extract a tubular shape, such as a blood vessel. The proposed method consists of a set of pairs of points. Each pair of points provides the Initial point and Target point for one geodesic. For each pair of Initial point and Target point, we calculate a special Riemannian metric with an additional *Radius* dimension to constrain the fast marching propagation so that our method can get a nice path without any shortcut. The given pairs of points can be easily obtained from a pre-segmented skeletonized image by any vessel detection filter like Hessian or Oriented Flux method. Experimental results demonstrate that our method can extract vessel segments at a finer scale, with increased accuracy.

1 Introduction

Automatic segmentation and analysis of vascular structures has been deeply developed during the last two decades[10]. Tubular structure enhancement filters, like Hessian based method[9] and Oriented Flux[13] are widely used methods. The response of those filters, named *vesselness* can be thresholded directly to extract the vessel boundaries and then apply a sequential thinning filter[12] to the binary vessel segmentation to obtain the vessel centrelines which can be further processed. Those centrelines sometimes are not exactly located in the middle of the tubular shape. And it is a difficult task to compute the width of the tubular shape from those binary segmented images.

In this paper, we deal with the problem of automatically finding a set of vessel segments by piecewise geodesics consisting of centreline positions and radii. The minimal path model has been improved deeply since the seminal Cohen-Kimmel model[5], in which tubular structures, or object edges are extracted as the form of geodesics or minimal paths. This classic minimal path model can lead to finding the global minimum with respect to a geodesic energy potential $\mathcal{P}$ between two given endpoints. The geodesic potential or metric can be isotropic[8, 7, 6] ($\mathcal{P}$ only depends on the pixel position), or anisotropic in the sense that path length depends on the path orientation as well[2, 3]. Once this potential is properly defined, Fast Marching methods[18, 16] are the favored methods to estimate geodesic distances, from which minimal paths can be extracted. However, for the minimal path models mentioned above, it is difficult for them to extract the centreline of the tubular structure and the local width information or boundaries simultaneously. In order to solve this drawback, Li and Yezzi[14] proposed a variant minimal path technique, which defines the potential domain $\mathbf{\Omega} \subset \mathbb{R}^{n+1}$, connected open and bounded, as the product of spatial space $\Omega \subset \mathbb{R}^n$ with a parameter space $]R_{min}, R_{max}[$ representing vessel radius collection. Thus, each point in the extracted path by [14] contains spatial position and the last dimension represents the vessel thickness at this spatial point, i.e, one point coordinate consists of spatial dimensions and one radius dimension. And the extracted path is also located on the centreline of the tubular structure with appropriate potential.

Unfortunately, Li and Yezzi model suffers from a drawback that they did not take advantage of vessel orientation information which plays an important role in vessel detection. Benmansour and Cohen[2] proposed to use an anisotropic Riemannian metric to enhance the Li and Yezzi model. In [2], the authors construct a multi-resolution Riemannian metric guiding the Anisotropic Fast Marching propagation in the domain $\mathbf{\Omega}$. Both [2] and [14] require the user to give two or more endpoints as the prior knowledge to track the minimal paths. In order to reduce the user input, several papers[1, 11, 15, 4] proposed to use keypoints searching method to detect recursively new start-points (keypoints) along the expected features by computing the curve length. But those methods require complicated stopping criteria.

The main purpose of this work is to introduce an automatic method to extract a complete tubular tree structure, such as the retinal vessel network, relying on the Benmansour-Cohen model[2] by using an Euclidean distance function to calculate the anisotropic metric for each initial vessel segment through thinning the thresholded vesselness image. The Euclidean distance function can constrain the anisotropic Fast Marching propagation and prevent shortcuts.

2 Background

In this paper, we only consider the 2D vessel segmentation so that one point $\mathbf{x} = (x, r) \in \mathbf{\Omega}$, where $x \in \Omega$ ($\Omega \subset \mathbb{R}^2$) denotes the point position in spatial dimensions and $r \in \ ]R_{min}, R_{max}[$ denotes the position in radius dimension.

2.1 Minimal Path

Let $\Im$ denote the collection of Lipschitz paths $\gamma : \ [0, L] \to \mathbf{\Omega}$. The weighted length through a geodesic energy potential $\mathcal{P}$ can be formulated as follows:

$$l_{\mathcal{P}}(\gamma) := \int_0^L \mathcal{P}(\gamma(s), \gamma'(s))\ ds\,, \tag{1}$$

where s is arc-length parameter and γ' denotes the tangent vector of path γ. The geodesic distance $\mathcal{U}_{\mathbf{s}}(\mathbf{x})$, or minimal action map, is the minimal energy of any path joining a point $\mathbf{x} \in \mathbf{\Omega}$ to a given initial point $\mathbf{s}$:

$$\mathcal{U}_{\mathbf{s}}(\mathbf{x}) := \min\{l_{\mathcal{P}}(\gamma) | \gamma \in \Im,\ \gamma(L) = \mathbf{x},\ \gamma(0) = \mathbf{s}\}. \tag{2}$$

The path $\mathcal{C}_{\mathbf{s},\mathbf{x}}$ is a *minimal path* if $l_{\mathcal{P}}(\mathcal{C}_{\mathbf{s},\mathbf{x}}) = \min_{\gamma}\{l_{\mathcal{P}}(\gamma),\ \gamma \in \Im\}$. There always exists at least one minimal path $\mathcal{C}_{\mathbf{s},\mathbf{x}}$.

2.2 Optimally Oriented Flux and Riemannian Metric Construction

The oriented flux[13] of an image $I : \Omega \to \mathbb{R}^2$, of dimension $d = 2$, is defined by the amount of the image gradient projected along the orientation $\mathbf{p}$ flowing out from a 2D circle at point x with radius r:

$$f(x; r, \mathbf{p}) = \int_{\partial \mathcal{C}_r} (\nabla(G_\sigma * I)(x + r\mathbf{n}) \cdot \mathbf{p})(\mathbf{p} \cdot \mathbf{n})\, ds\,, \tag{3}$$

where G_σ is a Gaussian with variance σ and $\mathbf{n}$ is the outward unit normal vector along $\partial\mathcal{C}_r$. ds is the infinitesimal length on the boundary of $\mathcal{C}_r$. According to the divergence theory, one has $f(x; r, \mathbf{p}) = \mathbf{p}^T \cdot \mathbf{Q}(x, r) \cdot \mathbf{p}$ for some symmetric matrix $\mathbf{Q}(x, r)$ whose eigenvalues and eigenvectors we denote by λ_i and $\mathbf{v}_i,\ i = 1, 2$ (Suppose that $\lambda_1 \leq \lambda_2$).

In this paper, as in Benmansour-Cohen model[2], the potential $\mathcal{P}(\gamma, \gamma')$ is set as a quadratic form with respect to a symmetric positive definite tensor $\mathcal{M}$ which is a 3×3 symmetric matrix:

$$\mathcal{P}(\gamma, \gamma') = \sqrt{\gamma'(.)^T \mathcal{M}(\gamma(.))\gamma'(.)}\ . \tag{4}$$

As described in [2], we consider only the orientations in the spatial dimensions. Thus $\mathcal{M}$ can be decomposed as follows:

$$\mathcal{M}(x, r) = \begin{pmatrix} \tilde{\mathcal{M}}(x, r) & \mathbf{0} \\ \mathbf{0} & \mathcal{P}_r(x, r) \end{pmatrix}. \tag{5}$$

The anisotropic entry $\tilde{\mathcal{M}}(x, r)$, which is a 2×2 symmetric definite positive matrix, at point $\mathbf{x} = (x, r)$ can be constructed by the eigenvectors $\mathbf{v}_1$ and $\mathbf{v}_2$ as:

$$\tilde{\mathcal{M}}(\mathbf{x}) = e^{\alpha \cdot \lambda_2(\mathbf{x})} \mathbf{v}_1(\mathbf{x}) \mathbf{v}_1(\mathbf{x})^T \ + \ e^{\alpha \cdot \lambda_1(\mathbf{x})} \mathbf{v}_2(\mathbf{x}) \mathbf{v}_2(\mathbf{x})^T\,. \tag{6}$$

The isotropic entry $\mathcal{P}_r(\mathbf{x})$ can be computed as:

$$\mathcal{P}_r(\mathbf{x}) = \beta \exp\left(\alpha \frac{\lambda_1(\mathbf{x}) + \lambda_2(\mathbf{x})}{2}\right), \tag{7}$$

where α controls the spatial anisotropic ratio defined as

$$\mu = \max_{(x,r) \in \mathbf{\Omega}} \sqrt{\exp\left(\alpha \cdot (\lambda_2(x, r) - \lambda_1(x, r))\right)}$$

while β controls the radius speed. For more details, we refer to [2].

2.3 Anisotropic Fast Marching Using Basis Reduction

Numerical methods for the minimal action map $\mathcal{U}_{\mathbf{s}}(\mathbf{x})$, see (2), introduce a discretization grid Z of $\mathbf{\Omega}$, and for each $\mathbf{x} \in Z$ a small mesh $S(\mathbf{x})$ of a neighborhood of $\mathbf{x}$ with vertices in Z (with the adequate modification if $\mathbf{x}$ is at or near the boundary). An approximation of $\mathcal{U}_{\mathbf{s}}$ is given by the solution of the following fixed point problem[16]: find $\mathcal{U}_{\mathbf{s}} : Z \to \mathbb{R}$ such that (i) $\mathcal{U}_{\mathbf{s}}(\mathbf{s}) = 0$ for the initial point $\mathbf{s}$, and (ii) for all $\mathbf{x} \in Z \setminus \mathbf{s}$

$$\mathcal{U}_{\mathbf{s}}(\mathbf{x}) = \min_{\mathbf{y} \in \partial S(\mathbf{x})} \mathcal{P}(\mathbf{x}, \mathbf{y} - \mathbf{x}) + \mathrm{I}_{S(\mathbf{x})} \mathcal{U}_{\mathbf{s}}(\mathbf{y}), \tag{8}$$

where $\mathrm{I}_{S(\mathbf{x})}$ denotes piecewise linear interpolation on a mesh $S(\mathbf{x})$. $\mathrm{I}_{S(\mathbf{x})}$ interpolates $\mathcal{U}_{\mathbf{s}}$ on $S(\mathbf{x})$ [2, 16, 20]. The expression (8) reflects the fact that the minimal path $\mathcal{C}_{\mathbf{s},\mathbf{x}}$, joining $\mathbf{x}$ to $\mathbf{s}$, needs to cross the stencil boundary $\partial S(\mathbf{x})$ at some point $\mathbf{y}$; hence it is the concatenation of a small path joining $\mathbf{x}$ to $\mathbf{y}$, of approximate length $\mathcal{P}(\mathbf{x}, \mathbf{y} - \mathbf{x})$, and of $\mathcal{C}_{\mathbf{y},\mathbf{x}}$, which energy is approximated by interpolation. A striking fact is that this N-dimensional fixed point system, with $N = \#(Z)$, can be solved in a single pass using the Fast Marching algorithm [20], provided the stencils $S(\mathbf{x})$ satisfy some geometric properties depending on the local geodesic potential $\mathcal{P}(\mathbf{x}, \cdot)$.

An adaptive construction of such stencils was introduced in [16], which led to breakthrough improvements in terms of computation time and accuracy for strongly anisotropic geodesic energy potentials, as in our application. It invokes Lattice Basis Reduction, a tool from discrete geometry which combines in an optimal way the geometric structure given by the Riemannian metric, and the arithmetic structure of the cartesian discretization grid.

2.4 Limitation of Classical Minimal Paths

Benmansour-Cohen model[2] can accurately extract the vessel boundaries and centrelines at the same time, and also very fast. Unfortunately, despite its numerous advantages, this model exhibits a disadvantage when applied to complete vessel network extraction such as retinal segmentation. It requires user provided endpoints at the end of each tubular structure end. This means expensive user intervention. For the keypoints method[1, 11, 15, 4], which requires less user intervention, there may be some missing tubular segments. This is mainly because of the loops in the tubular structure network.

To solve those problems, we propose a new method based on Benmansour and Cohen model with pre-segmented vessel map to automatically extract the tubular structure segments. Our method can be divided as follows: presegmentation, endpoints correction and constrained Fast Marching propagation. We will give details of those steps in the next section and a summary in Section 3.4.

3 The Proposed Constrained Piecewise Geodesics

3.1 Pre-Processing

In this paper, we use a vessel detector to filter the image and obtain a vesselness map. Then a constant threshold is applied to this vesselness map to get the binary segmented vessel image. In order to find the endpoints for each vessel segment, we thin the binary image by a sequential morphological filters[12] and remove all the branch points and crossover points. The entire skeleton is broken up into a set of segments, in which each segment consists of two endpoints. The branch or crossover points are defined as any skeleton point having at least three neighbors in 8-neighborhood system. Any endpoint is discovered if it has only one neighbor and segment point has two neighbors. In Fig. 1(c), we show the skeletons after applying thinning filter and the labeled segments in different colours in Fig. 1(d).

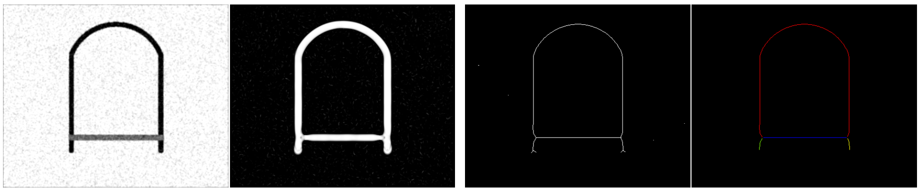

(a) (b) (c) (d)

Fig. 1. PreProcessing.(a) Original image. (b) Vesselness map computed by Hessian-based Filter[9]. (c) the Skeleton map of the image. (d) Label different segments with different colours after removing branch and crossover points

.

In our work, we firstly scan the entire skeleton image to find all the vessel segments with two endpoints and then label them. Delete the segments whose length in pixels are smaller than a given threshold T_{len}, but retain the segments who connect two branch or crossover points. Those segments will be stored in the set $\mathcal{T}$.

3.2 Constrained Riemannian Metric and Anisotropic Fast Marching

In the previous section, we have all the segments and the corresponding endpoints stored in $\mathcal{T}$. Each segment consists of two endpoints and all the segment points connected to the endpoints. For each segment $\hbar$ with two endpoints p_s and p_e, it is easy to extract the centerline by Benmansour-Cohen model[2] by taking one of the two endpoints as initial point and track the path from another one. However, sometimes shortcuts will occur and some segments will be missed. In Fig. 2(a), the extracted geodesic follows the segment labeled as blue in Fig 1(d).

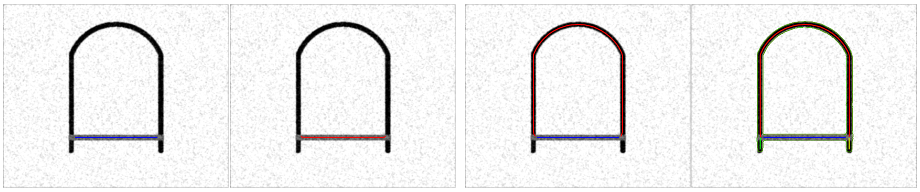

(a) (b) (c) (d)

Fig. 2. Results from Benmansour and Cohen model.(a) and (b) Extracted centrelines corresponds to the vessel segments labeled as blue and red in Fig. 1(d), respectively. (c) is the result of our method. (d) is the result of our method with endpoint correction (see text).

.

But the result in Fig. 2(b) is a short cut path. In order to solve this problem, we use the following function with respect to segment $\hbar \in \mathcal{T}$:

$$D_\hbar(x,r) = \begin{cases} 1, & \text{if } d_\hbar(x,r) \leq \ell\,; \\ +\infty, & \text{else} \ , \end{cases} \tag{9}$$

where ℓ is a given positive constant. And $d_\hbar(x,r)$ is a distance function:

$$d_\hbar(x,r) = \min_{x_\hbar \in \hbar} \|x - x_\hbar\|_2. \tag{10}$$

Note that (x,r) denotes a point in the domain $\mathbf{\Omega} = \Omega \times]R_{min}, R_{max}[$. Function $d_\hbar(x,r)$ represents the minimal Euclidean distance from spatial point $x \in \Omega$ to the segment $\hbar$. $D_\hbar$ in (9) gives a constraint volume computed by $d_\hbar$ and ℓ.

Based on (5), (9), and (10) we can construct the constrained Riemannian Metric for segment $\hbar \in \mathcal{T}$:

$$\mathcal{M}_\hbar = \begin{pmatrix} D_\hbar & \mathbf{0} \\ \mathbf{0} & D_\hbar \end{pmatrix} \begin{pmatrix} \tilde{\mathcal{M}} & \mathbf{0} \\ \mathbf{0} & \mathcal{P}_r \end{pmatrix} = \begin{pmatrix} (D_\hbar \cdot \tilde{\mathcal{M}}) & \mathbf{0} \\ \mathbf{0} & (D_\hbar \cdot \mathcal{P}_r) \end{pmatrix}. \tag{11}$$

In our method, in fact, distance $D_\hbar$ and $d_\hbar$ can be simply and fastly computed through applying the morphological dilation operation with radius ℓ to segment $\hbar$. Denote the dilated region as $\mathcal{R}_\hbar \subset \Omega$, $D_\hbar$ can be rewriten as:

$$D_\hbar(x,r) = \begin{cases} 1, & \text{if } x \in \mathcal{R}_\hbar\,; \\ +\infty, & \text{else}\,. \end{cases} \tag{12}$$

Combining the dilated region $\mathcal{R}_\hbar$ and $D_\hbar$, we use the Riemannian metric $\mathcal{M}$ in (5), instead of $\mathcal{M}_\hbar$ in (11). The detailed algorithm can be seen in Algorithm 1. In Algorithm 1, the input initial point $\mathbf{p}_s$ is defined in the domain $\Omega \times]R_{min}, R_{max}[$, i.e., $\mathbf{p}_s = (p_s,\, r_0)$ where $r_0 = 1$ which means one pixel length perimeter guess for $\mathbf{p}_s$. p_s and p_e are the two endpoints of segment $\hbar \in \mathcal{T}$.

In Algorithm 1 we give only a physical space endpoint p_e. Once the Fast Marching front meets one point $\mathbf{p} = (p_0, r)$ which follows $p_0 = p_e$, we consider $\mathbf{p} = (p_0, r)$ to be the endpoint. In Fig. 2(c), we demonstrate the result of our method. It can be seen that our method can overcome the shortcuts problem.

Algorithm 1 *ConstrainedAnisotropicFM*

Input: Metric $\mathcal{M}$, initial point $\mathbf{p}_s \in \boldsymbol{\Omega}$, endpoint $p_e \in \Omega$, dilated region $\mathcal{R}_\hbar \subset \Omega$.
Output: Paths $\mathcal{C}_\hbar$.
Initialization:
For each point $\mathbf{x} \in \boldsymbol{\Omega}$, set $\mathcal{U}(\mathbf{x})$=$+\infty$ and $\mathcal{V}(\mathbf{x}) =$ *Trial*.
Set $\mathcal{U}(\mathbf{p}_s)$=0.
Marching Loop:
1: Find $\mathbf{x}_{min} = (x_m, r)$, the *Trial* point which minimizes $\mathcal{U}$.
2: **if** $x_m \notin \mathcal{R}_\hbar$ **then**
3: Set $\mathcal{U}(\mathbf{x}_{min}) = +\infty$ and $\mathcal{V}(\mathbf{x}_{min})$ =*Accept*.
4: Return to 1.
5: **end if**
6: **if** $x_m = p_e$ **then** ▷ Stop the propagation.
7: Stop the Fast Marching Propagation and Track the minimal path $\mathcal{C}_\hbar$.
8: Output the path $\mathcal{C}_\hbar$.
9: **end if**
10: Tag $\mathbf{x}$ as *Accepted*. ▷ "Standard" fast marching.
11: **for** All $\mathbf{y}$ such that $\mathbf{x}_{min} \in S(\mathbf{y})$ and $\mathcal{V}(\mathbf{x}_{min}) \neq$ *Accepted* **do**
12: Compute $\mathcal{U}_{\text{new}}(\mathbf{y})$ using (8).
13: **if** $\mathcal{U}_{\text{new}}(\mathbf{y}) < \mathcal{U}(\mathbf{y})$ **then**
14: Set $\mathcal{U}(\mathbf{y}) \leftarrow \mathcal{U}_{\text{new}}(\mathbf{y})$
15: Set $\mathcal{V}(\mathbf{y})$=*Trial*.
16: **end if**
17: **end for**

3.3 Endpoints Correcting

Sometimes the endpoints of the segment $\hbar$ are not located at the exact center of the tubular structure. As an example, see the two endpoints of the segment in Fig. 1(d) labeled as red. This endpoint-bias will introduce inaccuracy to the extracted minimal paths around the initial point and endpoint (see the red path in Fig. 2(c)). In this section, we propose an endpoint correcting (EC) method to solve this problem before applying Algorithm 1. The proposed EC method relies on the Euclidean length $\mathcal{E}$ of the minimal path. We firstly introduce the Euclidean length calculation method during the Anisotropic Fast Marching propagation[4]: an approximation of $\mathcal{E}$ is the solution of the fixed point problem: find $\mathcal{E} : Z \to \mathbb{R}$ such that (i) for $\mathbf{p}_s \in \boldsymbol{\Omega}$, $\mathcal{E}(\mathbf{p}_s) = 0$, and (ii) for all $\mathbf{x} = (x_0, r_0) \in Z \setminus \mathbf{p}_s$, let $\mathbf{y}_\mathbf{x} = (y, r)$ be the point at which the minimum (8) is attained:

$$\mathcal{E}(\mathbf{x}) = \|y - x_0\|_2 + \mathrm{I}_{S(\mathbf{x})}\, \mathcal{E}(\mathbf{y}_\mathbf{x}), \tag{13}$$

Then a single pass solver is possible: whenever the Fast Marching updates $\mathcal{U}$, update $\mathcal{E}$ at the same time, by using the just computed minimizer $\mathbf{y}_\mathbf{x}$ from (8). In (13), the term $\|y - x_0\|_2$ is the Euclidean distance between y and x_0.

The EC method is described in Algorithm 2: for a given segment $\hbar \in \mathcal{T}$ and its two endpoints p_s, p_e we find its middle point $p_m \in \hbar$ and the dilated region $\mathcal{R}_\hbar$ with radius ℓ as input. Launch the Fast Marching from point $\mathbf{p}_m = (p_m, 1)$

Algorithm 2 *EndpointsCorrecting*

Input: Metric $\mathcal{M}$, endpoints p_s and p_e, initial point $\mathbf{p}_m$, dilated region $\mathcal{R}_\hbar \subset \Omega$.
Output: Paths $\mathcal{C}_\hbar$, new endpoints collection $\Phi_0 = \{\mathbf{p}_s, \mathbf{p}_e\}$.
Initialization:
For each point $\mathbf{x} \in \mathbf{\Omega}$, set $\mathcal{U}(\mathbf{x})$=$\mathcal{E}(\mathbf{x})$=$+\infty$ and $\mathcal{V}(\mathbf{x})$ = *Trial*.
Set $\mathcal{U}(\mathbf{p}_m)$=$\mathcal{E}(\mathbf{p}_m)$=0 and *RemainedEndpoints* = 2. Set point collection $\Phi = \varnothing$.
Marching Loop:
1: Find $\mathbf{x}_{min} = (x_m, r)$, the *Trial* point which minimizes $\mathcal{U}$.
2: **if** *RemainedEndpoints* = 0 **then**
3: Track the minimal path $\mathcal{C}$ from each point of Φ_0 and set $\mathcal{C}_\hbar = \mathcal{C}_\hbar \cup \mathcal{C}$;
4: Stop the algorithm completely.
5: **end if**
6: **if** $x_m \notin \mathcal{R}_\hbar$ **then**
7: Set $\mathcal{U}(\mathbf{x}_{min}) = \mathcal{E}(\mathbf{x}_{min}) = +\infty$ and $\mathcal{V}(\mathbf{x}_{min})$ =*Accept*.
8: Return to 1.
9: **end if**
10: **if** $x_m = p_e$ or $x_m = p_s$ **then**
11: *RemainedEndpoints* $\leftarrow$ *RemainedEndpoints* $- 1$;
12: **for** All $\mathbf{x} \in \mathcal{B}$ centred at $\mathbf{x}_{min}$ **do** ▷ Endpoints searching criteria.
13: **if** $\mathcal{E}(\mathbf{x}) \geq \big([\mathcal{E}(\mathbf{x}_{min})] + 1\big)$ and $\mathcal{V}(\mathbf{x})$ = *Accepted* **then**
14: Set $\Phi \leftarrow \mathbf{x}$.
15: **end if**
16: **end for**
17: **if** $\Phi \neq \varnothing$ **then**
18: Set $\Phi_0 \leftarrow \arg\min_{\mathbf{x}\in\Phi} \mathcal{U}(\mathbf{x})$
19: **else** Set $\Phi_0 \leftarrow \mathbf{x}_{min}$.
20: **end if**
21: **end if**
22: Tag $\mathbf{x}$ as *Accepted* and update $\mathcal{E}(\mathbf{x})$ using (13). ▷ "Standard" fast marching.
23: **for** All $\mathbf{y}$ such that $\mathbf{x}_{min} \in S(\mathbf{y})$ and $\mathcal{V}(\mathbf{x}_{min}) \neq$ *Accepted* **do**
24: Compute $\mathcal{U}_{\text{new}}(\mathbf{y})$ using (8);
25: **if** $\mathcal{U}_{\text{new}}(\mathbf{y}) < \mathcal{U}(\mathbf{y})$ **then**
26: Set $\mathcal{U}(\mathbf{y}) \leftarrow \mathcal{U}_{\text{new}}(\mathbf{y})$, $\mathcal{V}(\mathbf{y})$=*Trial*.
27: **end if**
28: **end for**

to propagate the weighted distance $\mathcal{U}$ and Euclidean distance $\mathcal{E}$ everywhere in $\mathbf{\Omega}$. Once either endpoint $\tilde{\mathbf{p}}_e = (p_e, r_e)$ is reached, search the desired point inside a set $\mathcal{B} : \{\mathbf{x} \in \mathbf{\Omega}, \|\mathbf{x} - \tilde{\mathbf{p}}_e\|_2 \leq r_{\mathcal{B}}\}$ according to the criteria described in Algorithm 2: We find a collection of points $\Phi := \{\mathbf{x}\,|\mathcal{E}(\mathbf{x}) \geq [\mathcal{E}(\tilde{\mathbf{p}}_e)]+1, \mathbf{x} \in \mathcal{B}\}$ where $[n]$ means the largest integer which is smaller than $n \in \mathbb{R}$. Then the desired endpoint can be selected as $\mathbf{p}_e = \arg\min_{\mathbf{x}\in\Phi} \mathcal{U}(\mathbf{x})$. After another endpoint with the same criteria is corrected, stop the algorithm completely. The criteria are based on the fact that among all the points with the same curve length λ, any point which is located at the centreline of the tubular structure has a local minimum arrival time. In Fig. 2(d), we show the results with the boundaries delineation. We can see the endpoints of red, green and yellow lines have been placed at the better positions compared with Fig. 1(d).

3.4 Summary of Our Method

In this section, we summaries our method as follows:

1. For a given image $I : \Omega \subset \mathbb{R}^2$, obtain its skeletonized image by removing all the branch and crossover points. Label each segment of the skeletonized image and store them in $\mathcal{T}$.
2. For each segment $\hbar \in \mathcal{T}$, do *EndpointsCorrecting* as described in Algorithm 2 to get a new set of segments $\mathcal{T}_{new}$.
3. For each segment $\hbar_{new} \in \mathcal{T}_{new}$, do *ConstraintAnisotropicFM* described in Algorithm 1 to obtain a set of minimal paths, in which each minimal path $\mathcal{C}$ consists of the centrelines and the radius value representing the vessel width.

4 Experiments

In Fig. 3(b) we shown a complete results obtained by the proposed method. The green lines represent the boundaries while the red lines are the centrelines of the vessel segments. It can be seen that our method can capture almost all the vessel segments without shortcuts. In this experiment, we set the anisotropic ratio $\mu = 15$, $\beta = 2$, the radius for the dilated region $\mathcal{R}_{\hbar}$ as 3.

In Fig. 3(a) we show the results by Benmansour-Cohen model. Fig. 3(c), (d) and (e) illustrate the details indicated by arrows. We can see that some vessel segments are missed because of shortcuts. As comparison, we show the result details of our method in Fig. 3(f), (g) and (h). In Fig. 4, we show the improved results after endpoints correcting. Yellow lines are the paths without endpoints correcting. Compared to the red lines which are produced after endpoints correcting, we can see the endpoints are located at more precise positions.

For evaluation we apply our method on 20 retinal images got from the test set of the DRIVE dataset[19], acquired through a Canon CR5 non-mydriatic 3CCD camera with a 45 degree field of view (FOV). We show the comparison between Benmansour-Cohen model[2] and our method in Table 1 with evaluation measure Accuracy, which can be computed by the ratio of the summation of the statistical components: the true positive and the true negative to the total number of pixels in the FOV[10]. In this paper, we erode the FOV region by 11 pixels to remove the effect of the boundaries of the FOV to the vessel pre-segmentation. We evaluate our results only inside this eroded FOV region. In Table 2 we show the computational time (CPU) of our algorithm in endpoints correcting and constrained Fast Marching respectively. We also compare the CPU with Benmansour-Cohen model[2] with the same given segment set. Our method can achieve almost 2 times faster than [2]. In this experiment, we use the parameters as: anisotropic ratio $\mu = 15$, $\beta = 1$, the radius for the dilated region $\mathcal{R}_{\hbar}$ equals 3.

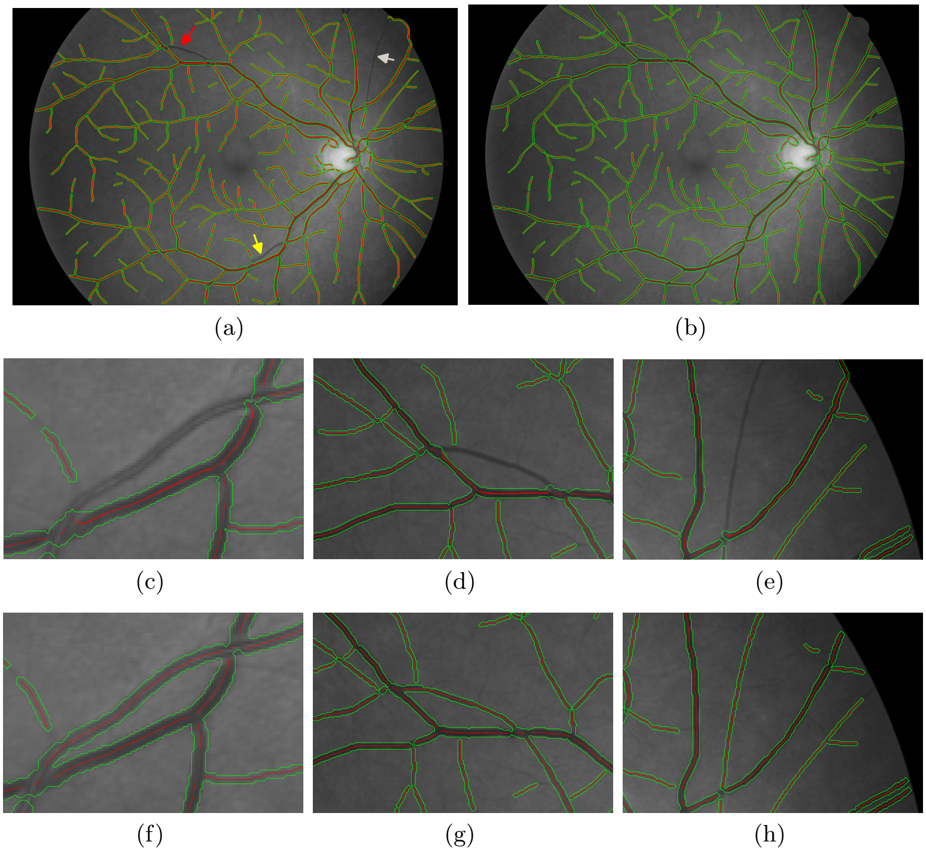

Fig. 3. Segmentation of a retinal image. (a) is the result by Benmansour and Cohen model and (b) is the result of our method (Green lines are the boundaries and red lines are the centrelines). (c-e) are the details of (a) indicated by arrows. (f-h) are the details shown in (b).

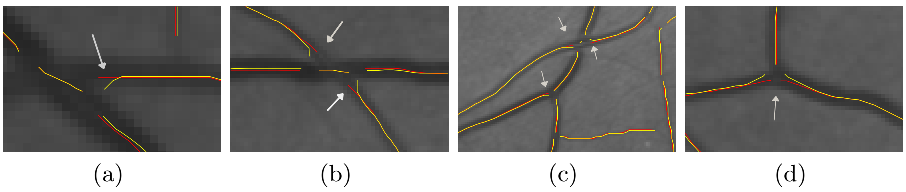

Fig. 4. Improved results by Endpoints Correcting. Yellow lines are the paths without Endpoints Correcting while red lines are the paths after Endpoints Correcting.

5 Conclusions

In this paper, we propose a new tubular structure extraction method based on the constraint anisotropic Fast Marching, and introduce a endpoints correcting

Table 1. Comparison of our segmentations with the second manual segmentation on the test set of DRIVE database.

Methods	Maximum	Minimum	Mean	Standard deviation
Benmansour-Cohen model[2]	0.947	0.9271	0.9372	0.0054
Proposed Method	0.949	0.9305	0.9397	0.0052

Table 2. Comparison of our segmentations CPU (in Seconds) with Benmansour-Cohen model[2] on 12 retinal images from DRIVE.

	Maximum	Minimum	Mean	Standard deviation
Benmansour-Cohen model	22.6	9.16	13.17	3.2
Endpoints Correcting	5.1	4.0	4.39	0.27
Constrained Fast Marching	5.6	4.4	5.06	0.353

method using Euclidean curve length. These ingredients allow our method to approximate piecewise minimal paths from complex tubular network, leading better extraction results compared to the classic Benmansour and Cohen model. Numerical experiments illustrate these improvements on several retinal images.

6 Acknowledgment

The authors thank Dr. Jean-Marie Mirebeau for helpful discussion about the Anisotropic Fast-Marching method. Also the authors would like to thank the suggestions and comments of anonymous reviewers.

References

1. Benmansour, F., Cohen, L.D.: Fast object segmentation by growing minimal paths from a single point on 2D or 3D images. Journal of Mathematical Imaging and Vision 33(2), 209–221 (2009)
2. Benmansour, F., Cohen, L.D.: Tubular Structure Segmentation Based on Minimal Path Method and Anisotropic Enhancement. International Journal of Computer Vision 92(2), 192–210 (2011)
3. Bougleux, S.., Peyré, G., Cohen, L.: Anisotropic Geodesics for Perceptual Grouping and Domain Meshing. In ECCV pp. 129–142 (2008)
4. Chen, D., Cohen, L., Mirebeau, J.M.: Vessel Extraction using Anisotropic Minimal Paths and Path Score. In Proc: ICIP pp. 1570–1574 (2014)
5. Cohen, L.D., Kimmel, R.: Global minimum for active contour models: A minimal path approach. International Journal of Computer Vision 24(1), 57–78 (1997)
6. Cohen, L.D.: Multiple Contour Finding and Perceptual Grouping using Minimal Paths. Journal of Mathematical Imaging and Vision 14(3), 225–236 (2001)
7. Cohen, L.D., Deschamps, T.: Grouping connected components using minimal path techniques. Application to reconstruction of vessels in 2d and 3d images. in Proc: IEEE CVPR (2001)

8. Deschamps, T., Cohen, L.D.: Fast extraction of minimal paths in 3D images and applications to virtual endoscopy. Medical Image Analysis 5(4), 281–299 (2001)
9. Frangi, A.F., Niessen, W.J., Vincken, K.L., Viergever, M.A.: Multiscale vessel enhancement filtering. In MICCAI pp. 407–433 (1998)
10. Fraz, M., Remagnino, P., Hoppe, A., Uyyanonvara, B., Rudnicka, A., Owen, C., Barman, S.: Blood vessel segmentation methodologies in retinal images - A survey. Computer Methods and Programs in Biomedicine 108(1), 130–137 (2012)
11. Kaul, V., Yezzi, A., Tsai, Y.: Detecting curves with unknown endpoints and arbitrary topology using minimal paths. IEEE Transactions on Pattern Analysis and Machine Intelligence 34(10), 1952–1965 (2012)
12. Lam, L., Lee, S.W., Suen, C.Y.: Thinning Methodologies - A Comprehensive Survey. IEEE Transactions on Pattern Analysis and Machine Intelligence 14(9), 869–885 (1992)
13. Law, M.W.K., Chung, A.C.S.: Three Dimensional Curvilinear Structure Detection Using Optimally Oriented Flux. In ECCV pp. 368–382 (2008)
14. Li, H., Yezzi, A.: Vessels as 4-D curves: Global minimal 4-D paths to extract 3-D tubular surfaces and centrelines. IEEE Transactions on Medical Imaging 26(9), 1213–1223 (2007)
15. Li, H., Yezzi, A.J., Cohen, L.D.: 3D multi-branch tubular surface and centerline extraction with 4D iterative key points. In MICCAI pp. 1042–1050 (2009)
16. Mirebeau, J.M.: Anisotropic Fast-Marching on cartesian grids using Lattice Basis Reduction. SIAM J. Numer. Anal. 52(4), 1573–1599 (2014)
17. Peyré, G., Péchaud, M., Keriven, R., Cohen, L.D.: Geodesic Methods in Computer Vision and Graphics, Foundations and Trends in Computer Graphics and Vision pp. 197–397 (2010)
18. Sethian, J.A.: Fast marching methods. SIAM Review 41(2), 199–235 (1999)
19. Staal, J., D.Abrámoff, M., Niemeijer, M., Viergever, M.A., Ginneken, B.V.: Ridge based vessel segmentation in color images of the retina. IEEE Transactions on Medical Imaging 23(4), 501–509 (2004)
20. Tsitsiklis, J.N.: Efficient algorithms for globally optimal trajectories. IEEE Transactions on Automatic Control 40(9), 1528–1538 (1995)